Role of Intramolecular Vibrations in Long-Range Electron Transfer between Pheophytin and Ubiquinone in Bacterial Photosynthetic Reaction Centers

Raffaele Borrelli, Mariangela Di Donato, and Andrea Peluso
Dipartimento di Chimica, Università di Salerno, I-84081 Baronissi, Salerno, Italy

ABSTRACT The dynamics of the elementary electron transfer step between pheophytin and primary ubiquinone in bacterial photosynthetic reaction centers is investigated by using a discrete state approach, including only the intramolecular normal modes of vibration of the two redox partners. The whole set of normal coordinates of the acceptor and donor groups have been employed in the computations of the Hamiltonian matrix, to reliably account both for shifts and mixing of the normal coordinates, and for changes in vibrational frequencies upon ET. It is shown that intramolecular modes provide not only a discrete set of states more strongly coupled to the initial state but also a quasicontinuum of weakly coupled states, which account for the spreading of the wave packet after ET. The computed transition probabilities are sufficiently high for asserting that electron transfer from bacteriopheophytin to the primary quinone can occur via tunneling solely promoted by intramolecular modes; the transition times, computed for different values of the electronic energy difference and coupling term, are of the same order of magnitude (10^2 ps) of the observed one.

INTRODUCTION

Long-range electron transfer (ET) is an important process in biosystems, being among the basic mechanisms for energy transduction in living systems (1,2). The basic concepts for understanding ET processes in condensed media have been provided by Marcus' theory (3) and its quantum extensions (4–6), which have found the physical factors that mostly affect ET rates. However, for understanding ET mechanisms at microscopic level—an important point for the design of biomimetic molecular machines able to reproduce in an efficient way important functions such as photosynthesis (7,8)—it is still necessary to explain how these physicochemical factors that drive ET are connected to the chemical properties of the redox partners and of their embedding medium. That is not an easy point; many ET processes are in fact experimentally very well characterized but mechanistically not so well understood, as testified by the fact that the physical factors that stabilize the long-living charge-separated state produced in the early ET steps in photosynthetic reaction centers (RC), a crucial point for the efficiency of the whole photosynthetic process, are not yet known; only a few hints can be found in the literature (9–11).

In a hierarchic order of the different effects that could affect ET dynamics in biosystems, the nuclear modes of vibrations of the two molecules that exchange an electron should be considered first. Thus, the knowledge of the vibronic levels of the two redox partners and of how they are coupled to each other should be the necessary starting point for any analysis intended to clarify both the structure-function relationships in long-range ET and the effects of specific interactions with the embedding medium. Unfortunately, this information was not easily available in the past and therefore in the majority of the articles dealing with ET dynamics the effect of the discrete set of intramolecular vibrational modes has been modeled by considering usually a single intramolecular mode, with a suitably averaged frequency. Although the high heuristic importance of such models, the assumption of a single quantum mode may pose limits to a deeper understanding of ET processes in biosystems. On the one hand such an approximation could compromise the ability of extracting from the experimental data important parameters, such as the electronic coupling element and the reorganization energy; on the other hand the assumption of only one or a few discrete modes makes it impossible to achieve the degeneracy conditions required for tunneling and, thus, it leads us to assign to the low-frequency motion of the surrounding medium a more important role than it might deserve.

In this article we report the results of a study of the dynamics of the elementary ET step from pheophytin (BPh) anion to primary ubiquinone (Q_A), occurring in bacterial photosynthetic RC (12), in which the parameters governing the vibrational motions have been entirely determined from the normal mode analyses of the two redox cofactors in their normal and reduced forms. Here we have resorted to computational means for the normal mode analysis, but all the important parameters used in the dynamics, i.e., the displacements between the equilibrium coordinates of the initial and final states and the normal mode frequencies, can be obtained from experimental data (13,14). We will pose most attention to the role of intramolecular modes of the two redox partners in ET dynamics, deliberately neglecting at

Submitted February 3, 2005, and accepted for publication May 4, 2005.

Address reprint requests to Andrea Peluso, E-mail: apeluso@unisa.it.

Raffaele Borrelli's present address is Centro Italiano Ricerche Aerospaziali, Capua, Italy.

0006-3495/05/08/830/12 $2.00

doi: 10.1529/biophysj.105.060574

this first stage the effects of the surrounding medium, with the purpose of understanding at what extent the intramolecular modes of the two moieties can drive long-range ET by themselves; on the basis of these preliminary results the possible role of low-frequency vibrations of the embedding medium can be better judged and, hopefully, modeled in a simpler way.

ET from BPh^- to Q_A is well suited to these purposes, because the ET rate is neither too fast nor too slow to infer a priori the involvement or not of intermolecular modes in the reaction mechanism. Indeed, pioneering works (15,16) have shown that the temperature dependence of ET rates for some elementary ET steps in RCs is modest, even when the Gibbs free-energy change upon ET is changed, suggesting, among other possible explanations, that high-frequency modes, which cannot be excited at room temperature, are involved in ET.

The hypothesis that intramolecular modes can drive ET by themselves has also been advanced in the last decade (17), on the basis of several investigations of photoinduced charge separation in covalently linked D-br-A systems in solution (D = donor, A = acceptor, br = bridge) (18), and was later confirmed by studies in supersonic jets under rigorous solvent-free conditions (17).

Long-living vibrational states, hundreds of picoseconds, have been found for certain excited vibrational states of a protein matrix (19), and the theoretical simulation of energy relaxation processes in myoglobin suggested that initially it takes place over a very limited number of states, initially proceeding via energy transfer to a couple of states that are in Fermi resonance with the initial state, without involving the huge number of low-frequency vibrational states of the protein (20).

Thus, on the basis of the above experimental findings, the analysis of ET dynamics by using a discrete state approach, posing attention on the intramolecular normal modes of the two redox partners, is justified and, hopefully, it could stimulate and guide further experimental work. Of course, such an analysis has to be performed by using realistic model systems of the acceptor and donor molecules. In this article we will apply a theoretical methodology, recently developed for studying nonradiative decays in photoexcited molecular systems (21), which, by using the whole set of normal coordinates of the two redox cofactors, allows for properly taking into account all the effects that can be important for ET: displacements of the equilibrium coordinates, mixing of the normal modes (Duschinsky effect), and changes in vibrational frequencies.

For the sake of clearness, in the next two sections we will discuss in detail the approximations used in the construction of the Hamiltonian matrix in its most general form, and the criteria used for choosing the normal modes of vibrations that are important in ET dynamics, even though nothing of new is added to the existing theory of radiationless transition (22). The results will show that for the BPh-Q_A pair the intramolecular modes of the two redox partners are sufficient to promote ET by themselves, on the condition that the electronic levels of the two redox partners are slightly scattered (by a thermal quantum k_bT) around their average value by thermal motion.

THE HAMILTONIAN MATRIX

Let us consider a supramolecular system characterized by L different molecular sites that can exchange an electron. For long-range ET in proteins, those sites can be considered in most of the cases as weakly coupled molecular entities, kept at fixed distances by a protein matrix, which at this stage we assume to be rigid. For simplicity in the notation, we will explicitly refer to a system with an unpaired electron that can be exchanged among closed shell molecular sites, but of course the same treatment can be applied also to cases where ET leads to a charge-separated diradical state. In such a supramolecular assembly there will be L low-lying diabatic electronic states, each of them corresponding to the mobile electron fully localized on one molecule. Let $|l\rangle$ denote the electronic state in which the unpaired electron is fully localized on the l-th molecule; because the electronic coupling is usually very weak, $|l\rangle$ can be chosen as the direct product of the eigenstates of the L electronic Hamiltonians of the noninteracting molecular units:

$$|l\rangle = \prod_{i=1}^{L} |il\rangle, \tag{1}$$

where the $|il\rangle$'s satisfy the set of time-independent Schrödinger equations:

$$H_i^{(el)}|il\rangle = U_{il}(\mathbf{Q}_{il})|il\rangle, \qquad i,l = 1,2\ldots L. \tag{2}$$

$U_{il}(\mathbf{Q}_{il})$ is the electronic energy of the i-th isolated molecular unit (with the unpaired electron localized on it if $i = l$) and $\mathbf{Q}_{il}$ its normal modes of vibration.

The vibrational basis functions $|\bar{v}_l\rangle$ for the l-th electronic state are then chosen as the direct product of the vibrational states of each molecular unit:

$$|\bar{v}_l\rangle = |\bar{v}_{1l}, \bar{v}_{2l}, \ldots \bar{v}_{Ll}\rangle = \prod_{i=1}^{L} |\bar{v}_{il}\rangle, \tag{3}$$

where $|\bar{v}_{il}\rangle$ is the set of vibrational eigenstates of the i-th isolated molecule in the l-th electronic state:

$$[T_i + U_{il}]|\bar{v}_{il}\rangle = E_{l,\bar{v}_{il}}|\bar{v}_{il}\rangle, \quad l = 1,2\ldots L, \quad i = 1,2,\ldots L, \tag{4}$$

T_i being the nuclear kinetic energy operator of the i-th molecular unit.

Throughout this article we will freeze rotations (we will consider molecules embedded in a protein matrix) and adopt harmonic approximation for the U_{il}'s:

$$U_{il} = \frac{1}{2}\mathbf{Q}_{il}^{\dagger}\boldsymbol{\omega}_{il}^{2}\mathbf{Q}_{il}, \tag{5}$$

where ω_{il} is the diagonal matrix of the vibrational frequencies of the normal modes of the i-th unit in the l-th electronic state. In the cases we will consider here, harmonic approximation is well suited because highly excited vibrational states will not be involved in ET dynamics, but for a displaced mode of Q_A; see infra. Anharmonic effects on this mode will be neglected at this stage but their inclusion is straightforward and does not pose any serious conceptual problem.

The Hamiltonian operator of the whole L-site system can then be written (23):

$$\mathcal{H} = \sum_{l,m}^{L} |l\rangle \mathcal{H}_{lm} \langle m|, \tag{6}$$

with:

$$\mathcal{H}_{lm} = \langle l|\mathcal{T}_N + \mathcal{H}_{el}|m\rangle, \tag{7}$$

where $\mathcal{T}_N$ and $\mathcal{H}_{el}$ include all the nuclear and electronic coordinates of the whole molecular assembly.

The total time-dependent vibronic wavefunction can be suitably expanded over a set of Born-Oppenheimer product wavefunctions:

$$\Psi(t) = \sum_{l,\bar{v}_l} \mathbf{C}_{\bar{v}_l}(t)|l, \bar{v}_l\rangle. \tag{8}$$

Because of the harmonic approximation introduced before, the basis states $|il\rangle$ are known in spectroscopist notation as crude adiabatic electronic wavefunctions, inasmuch as their dependence on the nuclear coordinates is neglected; nonetheless crude adiabatic approximation can be a very good starting point for the analysis of potential energy surfaces (24).

The expansion coefficients $\mathbf{C}_{\bar{v}_l}(t)$ of Eq. 8 are determined by solving the time-dependent Schrödinger equation:

$$-i\hbar \begin{pmatrix} \dot{\mathbf{C}}_{\bar{v}_1}(t) \\ \dot{\mathbf{C}}_{\bar{v}_2}(t) \\ . \\ . \\ \dot{\mathbf{C}}_{\bar{v}_L}(t) \end{pmatrix} = \begin{pmatrix} \mathbf{H}_{11} & \mathbf{H}_{12} & . & . & \mathbf{H}_{1L} \\ \mathbf{H}_{12}^{\dagger} & \mathbf{H}_{22} & . & . & \mathbf{H}_{2L} \\ & . & . & . & \\ & . & . & . & \\ \mathbf{H}_{1L}^{\dagger} & \mathbf{H}_{2L}^{\dagger} & . & . & \mathbf{H}_{LL} \end{pmatrix} \begin{pmatrix} \mathbf{C}_{\bar{v}_1} \\ \mathbf{C}_{\bar{v}_2} \\ . \\ . \\ \mathbf{C}_{\bar{v}_L} \end{pmatrix}, \tag{9}$$

with initial conditions specifying the initial state of the system. Each $\mathbf{H}_{lm}$ in Eq. 9 is a matrix whose size depends on the number of vibrational states of the l-th and m-th electronic state that are assumed to be active in ET dynamics (in our terminology an active mode is a mode that can change its quantum number for effect of a transition from one electronic state to another). Accordingly, the $\mathbf{C}_{\bar{v}_i}$'s are column vectors, whose size is given by the number of vibrational states of the i-th electronic state.

As concerns the diagonal blocks of the Hamiltonian matrix, their computation in harmonic approximation is straightforward; the $\mathbf{H}_{ll}$ are in fact diagonal matrices, whose elements are simply given by the eigenenergies of multidimensional harmonic oscillators. By denoting with $n_{i,\,lk}^{(\alpha)}$ the vibrational quantum number of the α-th normal mode of the i-th molecular unit in the lk-th vibronic state, the diagonal elements take the form:

$$H_{lk,lk} = \sum_{i=1}^{L} \left[\sum_{\alpha}^{3N_i-6} \hbar n_{i,lk}^{(\alpha)} \omega_{i,lk}^{(\alpha)} \right], \tag{10}$$

where the index i runs over all the molecular units and α over all the normal modes of the i-th unit. The zero point energy does not appear in Eq. 10 because its contribution can be conveniently included in the electronic energy term.

Because the $|il\rangle$'s defined by Eq. 2 are not true diabatic states, those for which kinetic couplings are zero (25), both the nuclear kinetic energy and the electronic operators will contribute to the electronic coupling element. We will neglect the former contribution and we will further assume that the dependence of the electronic couplings on the nuclear coordinates can be neglected. That is a good approximation for the cases we are dealing with, because the displacements between the equilibrium nuclear configurations of $|il\rangle$ and $|im\rangle$ ($l \neq m$) are small (see infra), and therefore ET will take place in a very limited region of the nuclear coordinates, within which the $\mathbf{Q}$ dependence of the electronic couplings can be safely neglected. However, it must be remarked that in some specific cases, not this one, the symmetry of the system obliges us to consider the nuclear dependence of the electronic coupling element, in particular when the coupling mode is not a totally symmetric one and symmetry is conserved in the radiationless transition (see Borrelli and Peluso (21) and references therein).

With the above assumptions, after integration over the electronic coordinates, the coupling terms between the vibronic states of $|l\rangle$ and $|m\rangle$ are given by:

$$H_{l\bar{v}_l,m\bar{v}_m} = H_{lm} \times \langle \bar{v}_{ml}|\bar{v}_{mm}\rangle \langle \bar{v}_{ll}|\bar{v}_{lm}\rangle \times \prod_{i\neq l,m} \delta_{\bar{v}_{il},\bar{v}_{im}}, \tag{11}$$

where $H_{lm} = \langle ll|\mathcal{H}^{el}|mm\rangle$ is the electronic coupling term, and $\langle \bar{v}_{ml}|\bar{v}_{mm}\rangle$ and $\langle \bar{v}_{ll}|\bar{v}_{lm}\rangle$ are the multidimensional Franck-Condon integrals over the normal modes of the two molecular units involved in the $l \rightarrow m$ nonradiative transition.

The basic ingredients to build up the Hamiltonian matrix that determines the time evolution of the system are therefore: i), the relative energy of the L vibronic ground states (including the zero point contribution), which are usually available from spectroscopic measurements; ii), the normal modes of each electronic states, which according to the above assumptions can be evaluated for each isolated molecule, cf. Eq. 3; iii), the electronic coupling term H_{lm}, which can be estimated by empirical expressions or computed from the splitting of the two electronic states in the avoided crossing region (4,26); iv), the Franck-Condon integrals, namely the probability amplitude for the vibrational states of l-th electronic state to be found in those of the m-th electronic state.

The assumption at point (*ii*) neglects the possible effects of the interaction of the redox cofactors with the protein matrix. These effects could be included by resorting to hybrid quantum mechanics/molecular mechanics approaches. At this first stage, we have preferred to keep things as simple as possible, in view of the fact that small changes in the computed frequency, due to van der Waals contacts or H-bonds with the matrix atoms, cannot significantly affect ET dynamics. That is because, in these weakly coupled systems, the couplings between initial and final states are dominated by the displacements of the equilibrium positions of the normal and reduced forms of the redox cofactors, the contribution due to frequency changes upon ET being negligibly small. The effect of the protein matrix upon the equilibrium configurations of the redox cofactors is not expected to be significant, at least in the case we are dealing with, because the largest displacement, cf. Table 1, is roughly 0.1 Å, delocalized on the whole quinone molecule.

Choice of the active modes for ET

In the discrete state approach to ET dynamics, the selection of the vibrational states to be used in the time evolution is probably the most important problem to deal with. There are two factors that determine the involvement of a given state in the dynamics of the system: the energy and its couplings with the initial state and with other states that can be populated in the time evolution of the system. The coupling between two states can be either direct or indirect, i.e., mediated by a third state, whose energy can be outside the range in which vibrational states can be effectively populated. Because of the indirect couplings, the criterion purely based on the selection of a small energy range can only be used as a first filter for selecting those states that can be populated in time, but in dynamics all their couplings with vibronic states falling at higher or lower energy must be considered. Because the density of states of large protein cofactors hugely increases with the energy (see infra (Fig. 2)) the problem would rapidly become unsolvable as the energy difference between the vibronic ground states of the initial and final states increases.

In the computational scheme outlined above, the difficulty given by indirect couplings is minimized (completely avoided in the case of only two electronic states) by using a basis of oscillators for each electronic state, so that all the $\mathbf{H}_{ii}$ of Eq. 9 are diagonal matrices. Furthermore, the use of such a basis offers also the advantage that the most coupled modes can be determined by projecting the normal modes of one electronic state into those of the other. In fact, only those modes that are either displaced or mixed each other for the effect of the electronic transition $|l\rangle \rightarrow |m\rangle$ can change their quantum numbers during the time evolution of the system, all other modes will be frozen in their initial quantum state, because changes in quantum numbers would make the Franck-Condon integrals, and therefore the whole coupling with the initial state, vanishingly small.

TABLE 1 Wavenumbers (cm^{-1}), dimensionless displacements, and mixing coefficients of the most displaced or mixed normal modes of the pair Q_A/Q_A^-

Mode*†	Frequency		K	J‡
	Q_A	Q_A^-	$Q_A \rightarrow Q_A^-$	
1	24.22	76.41	0.313	0.29(1) − 0.44(2) + 0.75(3) + 0.23(5) + 0.31(6)
2	42.37	86.16	−0.260	0.83(1) + 0.17(2) − 0.31(3) + 0.41(5)
3	75.06	93.16	−0.018	0.85(2) − 0.51(3)
4	89.98	128.06	0.338	0.28(1) + 0.83(4) − 0.46(5)
5	117.98	149.70	0.176	0.37(1) + 0.54(4) + 0.75(5)
9	277.93	318.45	0.324	–
12	375.15	367.50	−0.572	–
13	420.39	420.77	−0.145	0.74(13) + 0.64(14)
14	423.84	447.12	−0.151	−0.65(13) + 0.74(14)
15	460.29	473.29	1.629	–
19	649.67	667.61	0.254	–
30	1179.79	1174.46	0.783	–
32	1227.58	1220.39	−0.346	–
41	1529.68	1521.06	0.461	–
45	1723.79	1545.19	0.708	–
46	1729.29	1643.85	0.803	–
49	3147.93	3074.42	−0.002	−0.72(49) + 0.64(50) + 0.15(51) − 0.16(52)
50	3152.00	3076.30	0.007	0.66(49) + 0.73(50)
51	3183.81	3121.07	−0.001	−0.16(49) + 0.16(50) − 0.65(51) + 0.73(52)
52	3187.81	3121.18	−0.002	0.74(51) + 0.66(52)

*Only modes with displacement longer than 0.1.
†Only mixed modes with maximum coefficient lower than 0.85.
‡Numbers in parentheses refer to the modes of Q_A^-.

The displaced and mixed modes, which therefore are the ''active'' modes in dynamics, can be determined by the affine Duschinsky's transformation (27);

$$\mathbf{Q}_l = \mathbf{J}\,\mathbf{Q}_m + \mathbf{K}, \tag{12}$$

where $\mathbf{Q}_l$ and $\mathbf{Q}_m$ are the normal mode vectors of $|l\rangle$ and $|m\rangle$, $\mathbf{J}$ is the rotation matrix, and $\mathbf{K}$ the displacement vector. Actually, because the vibrational wavefunction is factorized (cf. Eq. 3) only the normal modes of the two molecules that exchange an electron will really matter, the modes of all the other units being unchanged.

The rotation matrix $\mathbf{J}$ and the displacement vector $\mathbf{K}$ can be easily determined once the equilibrium geometries and the normal modes of the two electronic states are known (28,29).

Duschinsky's affine transformation is also the starting point for evaluating multidimensional Franck-Condon integrals; there are several procedures in the literature to compute Franck-Condon integrals (30,31); we have used that of Peluso et al. (30), implemented in the computer program MOLFC (32).

Noteworthy, Eq. 12 holds exactly only for small displacements of the normal coordinates. It can happen that a rotation of a side substituent makes a component of the $\mathbf{K}$ vector very large. To our opinion in this case it is better to project out the large amplitude mode and treat it with an anharmonic potential, restricting the computation of the FC integrals to all the other modes.

Energy parameters and electronic coupling elements

The Gibbs free-energy change for ET from BPh^- to Q_A is 0.62 eV (33). That value is probably not entirely related to ET, but it could include terms due to the stabilization of the Q_A^- by the surrounding groups, which, according to a few experimental pieces of evidence, takes place after ET has occurred. Kinetic studies have provided evidence in favor of a temperature-dependent extra stabilization of the $P^+Q_A^-$ state, which can be either due to solvent reorganization energy—there is evidence of conformational changes on microsecond timescale that may solvate Q_A^- (34,35)—or to chemical processes occurring at the Q_A site, probably involving proton movements around Q_A (36,9). There is uncertainty about the amount of energy to be assigned to those extra-stabilization processes; it should vary in the range 0.2–0.35 eV, the former value being suggested by photoacoustic measurements (34), the latter one by ab initio computations of the energy gain for proton transfer from the H-bonded iron histidine to Q_A^- (9). We have therefore explored a few values of the energy difference between the initial and final electronic states, ΔE_{el}, ranging from 0.62 to 0.25 eV.

As concerns the electronic coupling element, both the size of the system and the lack of symmetry, which can be very helpful in computing the electronic coupling element, rule out the possibility of computing that parameter by ab initio or semiempirical configuration interaction (CI) computations. A reliable estimate can however be obtained from the widely accepted exponential dependence of the electronic coupling element with the distance between the donor and acceptor site. We have used Hopfield's expression (4):

$$H_{lm} = \frac{2.7}{\sqrt{N_a N_b}} \exp(-\beta R_{lm}) \qquad \text{in eV}, \tag{13}$$

where R is the edge-to-edge distance between two large aromatics of N_a and N_b atoms.

The x-ray structure of the photosynthetic RC from *Rhodobacter sphaeroides* (37) indicates that the edge-to-edge distance between BPh and Q_A is ~9.3 Å. The parameter β has been estimated by taking as a reference the values of the electronic coupling elements between quinones in bacterial photosynthetic RC, evaluated as half of the energy difference of the two adiabatic states in a point of the avoided crossing region, both at ab initio multireference configuration interaction (MRCI) and semiempirical MNDO/AM1/CI level of computations (38). The ab initio MRCI value (17 cm^{-1}) yields $\beta = 0.49$ $Å^{-1}$, a lower value than that suggested by Hopfield (0.72) (4) but in line with other values reported in the literature (39), whereas the semiempirical result (4 cm^{-1}) leads to $\beta = 0.58$. The resulting coupling factor for ET between BPh and Q_A are ~30 and 13 cm^{-1}, respectively, the latter one in good agreement with Kuhn's estimate (10 cm^{-1}), obtained by evaluating the coupling element between the highest occupied and the lowest unoccupied molecular orbitals of the donor and acceptor groups in the Slater potential field (40).

RESULTS

Active modes and Franck-Condon integrals

The components of the $\mathbf{K}$ vector and the coefficients of the $\mathbf{J}$ matrix for the most displaced and mixed modes of the pair Q_A/Q_A^- are reported in Table 1. The most displaced mode is the symmetric CO stretching coupled to a ring breathing motion, falling at 460 (473 for Q_A^-) cm^{-1} ($K = 1.629$). Apart from this mode, which was the only one really important in our previous computations of ET dynamics between benzoquinones (38), for the native ubiquinone the presence of methoxy groups determines the appearance of several low-frequency modes, whose equilibrium positions are significantly displaced. These modes should significantly increase the Franck-Condon (FC) weighted density of states and therefore they will be included in dynamics.

In the high-frequency region there are also several modes whose displacements are significant (higher than 0.1). These modes will be important for ET from the BPh to Q_A, because of the large electronic energy gap to be filled up.

As concerns Duschinsky effect, there are three groups of significantly mixed modes. The first group includes modes that are also displaced and therefore most of them will be considered as active modes in dynamics. The second group includes a pair of modes with $\omega \approx 420$ cm^{-1}, whose FC integrals rapidly vanish as the difference in quantum numbers of the initial and final vibronic states increases. We will therefore consider these modes as potentially active modes in dynamics, but with a low level of excitation ($\Delta n = 1$). The last group of mixed modes, consisting of high frequency C-H stretching modes, gives rise to very low FC integrals and therefore will be discarded.

The most displaced modes of the BPh^-/BPh pair are reported in Table 2. There are several modes whose equilibrium positions are displaced upon extraction of the unpaired electron from the anion radical, but only for a few of them the displacement is significant (see infra), and there is a large number of mixed modes. There are four groups of strongly mixed modes; for two of them, those falling at lowest frequency, the elements of the **J** matrix have been reported in Table 2. The other two groups include eight modes, from 1088 and 1191 cm^{-1}, and 13 modes, falling in the wavenumber range 1327–1509 cm^{-1}, both exhibiting mixing coefficients of the same order of magnitude as those reported in Table 2. It is not possible to consider all these mixed modes as active modes in ET dynamics, but, as it will be seen, the transition probabilities for ET from BPh^- to Q_A are sufficiently high even when the higher-frequency mixed modes are not allowed to change their vibrational quantum numbers in the radiationless transition.

In Fig. 1 the FC integrals between the ground vibrational initial state and a manifold of selected final states for the $|BPh^-Q_A\rangle_{\bar{v}=0} \rightarrow |BPhQ_A^-\rangle_{\bar{v}}$ transition are reported as a function of the vibrational energy of the final state, in the energy range where experimental results indicate that the transition occurs. The space of the active modes, those which are allowed to change their quantum numbers during the transition, includes all the most displaced modes of both BPh and Q_A and a small fraction of mixed modes, the list of active modes is given in the figure caption. About 250×10^6 (close to the present upper limit of the MOLFC package) FC integrals have been computed and only those higher than 1×10^{-4} have been reported. Although several mixed modes and many displaced modes have been frozen in their ground state, the plot of Fig. 1 shows a quasicontinuum of states that are coupled with the initial ground state. Fig. 1,

TABLE 2 Wavenumbers (cm^{-1}), dimensionless displacements, and mixing coefficients of the most displaced or mixed normal modes of the pair BPh^-/BPh

Mode*†	Frequency		K	$J^‡$
	BPh^-	BPh	$BPh^- \rightarrow$ BPh	
1	28.41	32.63	0.001	0.64(1) + 0.68(2) + 0.16(3) − 0.15(4) + 0.23(5) − 0.15(7)
2	34.45	48.46	0.000	−0.76(1) + 0.57(2) + 0.11(3) − 0.15(4) + 0.22(5)
3	57.45	67.36	−0.001	0.40(2) − 0.14(3) + 0.52(4) − 0.73(5)
4	67.44	70.02	0.000	−0.14(2) + 0.96(3) − 0.20(5)
5	74.34	81.45	−0.004	0.82(4) + 0.55(5)
6	94.73	108.98	−0.098	–
9	135.38	135.48	0.355	–
10	146.60	146.22	0.884	–
18	275.98	277.64	0.358	–
29	540.44	529.85	0.266	–
41	731.90	730.64	0.262	–
46	794.93	810.15	−0.250	0.71(47) − 0.43(48) 0.52(54) − 0.10(57) + 0.11(58)
47	805.52	814.75	−0.250	→ 46
48	810.86	834.01	0.000	−0.37(47) − 0.44(48) + 0.20(50) + 0.50(51) + 0.18(54) + 0.56(55)
49	823.66	839.86	0.018	0.48(47) + 0.50(48) + 0.43(50) + 0.43(51) − 0.27(54) + 0.21(55)
50	830.85	842.93	0.000	−0.18(47) + 0.52(48) − 0.15(50) + 0.19(51) 0.74(54) − 0.23(58)
51	832.02	844.88	0.000	→ 49
52	837.68	863.70	−0.090	0.64(50) − 0.59(51) + 0.21(54) + 0.16(55) + 0.20(57) − 0.30(60)
53	851.35	865.04	−0.028	0.13(47) + 0.19(48) − 0.32(50) − 0.33(51) + 0.73(55) − 0.40(57)
54	852.54	867.25	0.000	0.82(52) − 0.56(53)
55	857.43	882.85	0.000	−0.55(52) − 0.82(53)
57	875.63	904.07	0.000	+0.21(48) + 0.14(51) + 0.12(54) − 0.29(57) + 0.88(58)
58	886.48	916.30	0.000	→ 56
78	1184.40	1204.92	−0.248	–
101	1454.20	1473.73	−0.268	–
114	1654.03	1658.35	0.289	–
115	1669.83	1673.17	−0.304	–

*Only modes with displacement longer than 0.25.
†Only mixed modes with maximum coefficient lower than 0.85.
‡Numbers in parentheses refer to the modes of BPh.

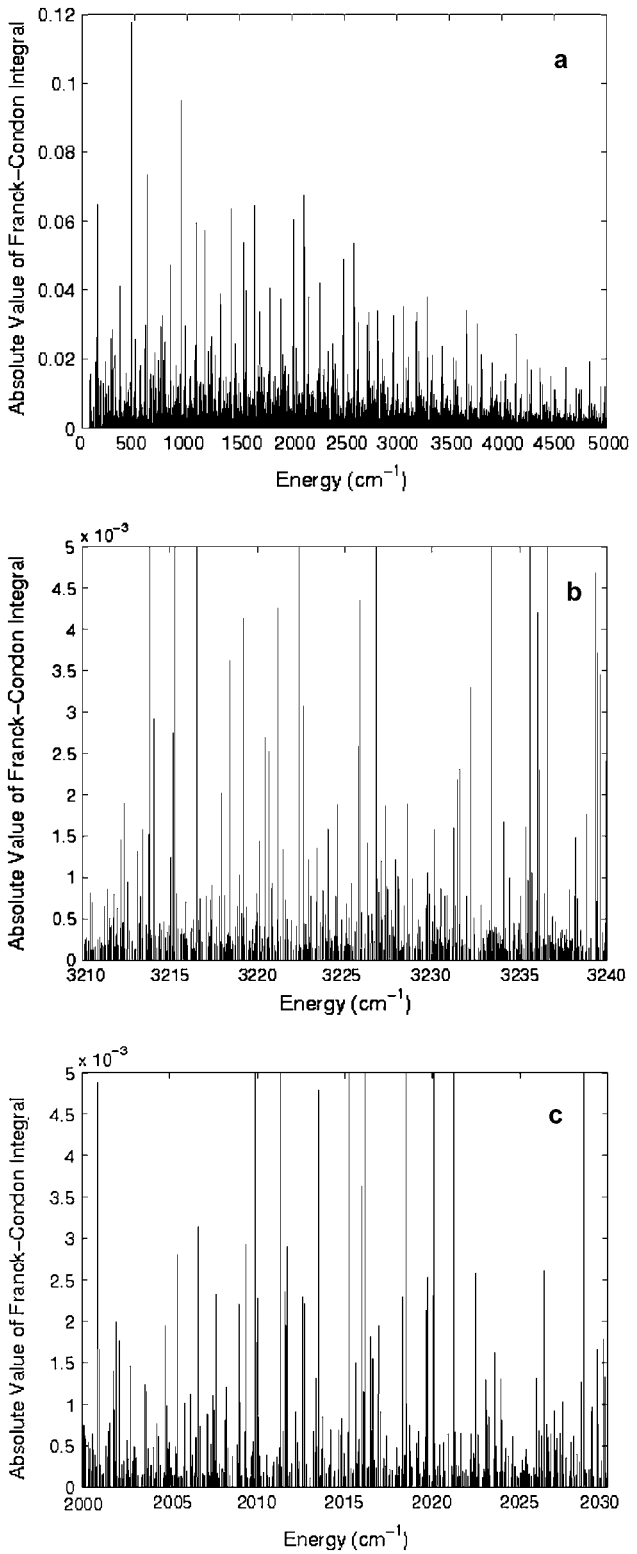

FIGURE 1 Franck-Condon integrals as a function of the vibrational energy difference for the transition: $|\mathrm{BPh}^{-}\mathrm{Q_A}\rangle_{\bar{v}=0} \rightarrow |\mathrm{BPhQ_A^{-}}\rangle_{v}$. Wavenumbers ($\mathrm{cm}^{-1}$) and number of states for each oscillator (in parentheses) of the excited modes: {32.63(2), 48.46(2), 67.36(2), 70.02(2), 135.48(3), 146.22(5), 277.64(2), 730.64(2), 76.41(3), 86.16(3), 93.16(2), 128.06(3), 149.70(3), 206.90(2), 318.45(3), 367.50(3), 473.29(5), 1174.46(3), 1545.19(3), 1643.85(2)}.

b and *c*, are magnifications of Fig. 1 *a* over a much smaller energy interval around $\Delta E_{\mathrm{el}} = 0.25$ and 0.4 eV (two values that will be investigated in dynamics), showing the existence of a quasicontinuum manifold of vibrational states even in such a tiny energy interval.

The largest FC integrals occur in the region 1000–2500 cm^{-1}, because that energy region is accessible by putting one quantum on a few displaced modes, beyond 2500 cm^{-1} more quanta are needed and therefore the FC integrals slowly go down. However, as concerns the ET rate it must be considered that the decrease of the FC integrals is counterbalanced by the strong increase in the total density of states (see Fig. 2) so that, although more weakly coupled, there are much more vibrational states coupled with the initial state.

With the data of Tables 1 and 2 the intramolecular reorganization energy:

$$\lambda = \frac{1}{2}\sum_{\mathrm{i}} \hbar\omega_{\mathrm{i}} K_{\mathrm{i}}^{2}, \tag{14}$$

(K_{i} = dimensionless displacement) can be easily computed. The total reorganization energy, computed by summing over all modes, is ~0.41 eV, ~0.3 eV from $\mathrm{Q_A}$ and 0.1 eV from BPh. The total reorganization energy yielded by DFT/B3LYP computations is 0.40 eV, testifying the reliability of the adopted harmonic approximation. The reorganization energy obtained by Eq. 14 by summing over only the modes included in dynamics (cf. caption of Fig. 3) is 0.27 eV. The most displaced mode of $\mathrm{Q_A^{-}}$ (473 cm^{-1}) contributes to half of the whole reorganization energy of $\mathrm{Q_A^{-}}$, whereas for BPh, there are no modes whose contributions predominate.

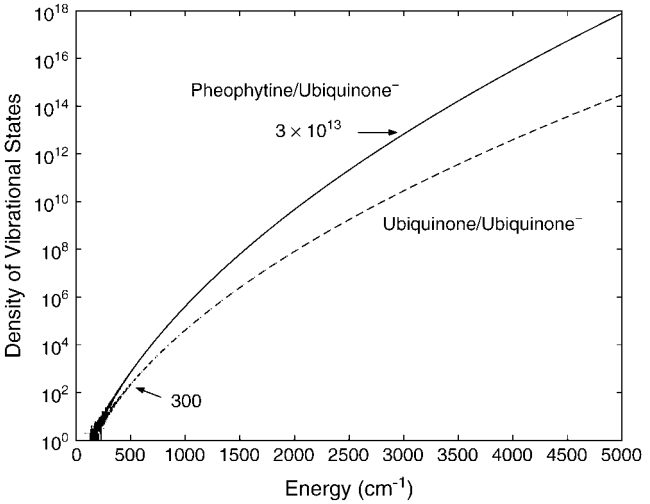

FIGURE 2 Total density of states versus energy for the pair pheophytin/ubiquinone anion, computed by using the Beyer-Swinehart algorithm (60,61), and the vibrational frequencies computed at DFT level. The case of the pair ubiquinone/ubiquinone anion is also reported for showing the huge difference between these two long-range ET processes in photosynthetic RC.

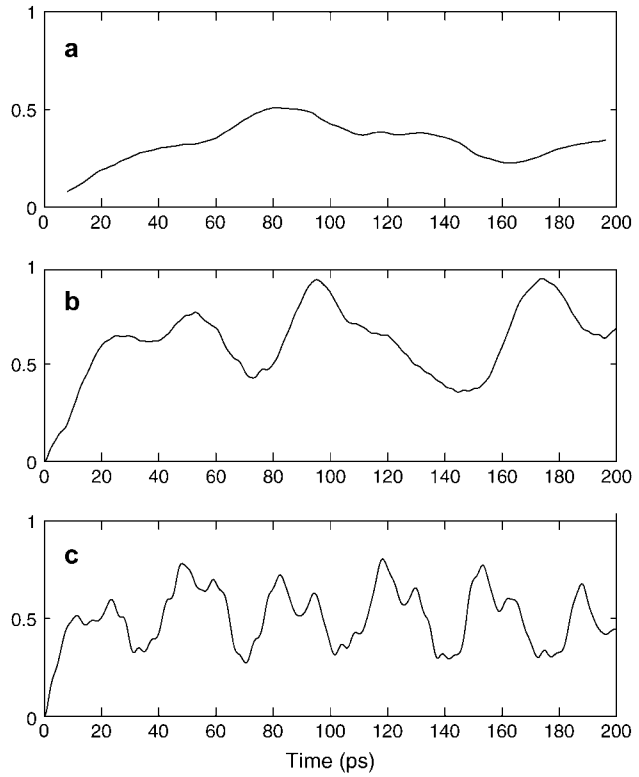

FIGURE 3 Transition probabilities of ET from pheophytin to ubiquinone: $\Delta E_{el} = 0.62$ eV (*a*), 0.40 eV (*b*), 0.25 eV (*c*); electronic coupling element: 30 cm^{-1}. Frequency of excited vibrations and number of states for each oscillator (in parentheses): (*a* and *b*) pheophytin 98(3), 135(3), 146(3), 277(3), 529(2), 730(2), ubiquinone 76(3), 86(3), 128(3), 318(3), 367(3), 473(5), 1174(3), 1545(3), 1643(3); (*c*) pheophytin 135(3), 146(3), 529(3), 730(3), 1184(3), ubiquinone 76(3), 86(3), 128(3), 318(3), 367(3), 473(5), 1174(2), 1545(2), 1643(2).

Transition probabilities

The Franck-Condon integrals reported in Fig. 1 show that there is a dense manifold of final vibronic states that are weakly coupled to the initial ground vibronic state and a more sparse set of more strongly coupled states. The former set of states could be too weakly coupled to promote long-range ET, we have therefore first investigated to what extent transition probabilities are affected by small change in ΔE_{el}, by performing several time propagations of the wavefunction within an energy range of ± 25 cm^{-1}, about a thermal quantum at 35 K, around three possible values of the electronic energy difference, namely 0.62, 0.4, and 0.25 eV. In no case the transition probabilities dropped below one-fourth of the maximum value obtained in each energy range, without attempting to optimize the active space for each energy point. This ensures that the computed transition probabilities are not due to the occurrence of a few accidental degeneracies, but rather to the existence of a Franck-Condon weighted density of states sufficiently large to promote ET.

The transition probabilities for ET from the ground vibronic state of $|BPh^{-}Q_A\rangle$, summed over the vibrational manifold of $|BPhQ_A^{-}\rangle$ and averaged with respect to energy fluctuations (Boltzmann weights), are reported in Fig. 3, for the three adopted values of ΔE_{el}; the electronic coupling element has been set to 30 cm^{-1}. The active space included the most displaced modes of BPh and Q_A^{-}; see the caption of Fig. 3 for more details.

In all the cases transition probabilities are high, approaching unity for $\Delta E_{el} = 0.25$ and 0.4 eV. In the case of $\Delta E_{el} = 0.62$ eV the maximum probability is ~0.6, but for such a high value of the electronic energy difference between the initial and final diabatic states there are many other vibrations that should be included in the active space. At this stage, the maximum number of states allowed in computations is $\sim 2 \times 10^8$, the bottleneck being the storage of the FC integrals.

Inspection of Fig. 3 shows that transition times increase as the electronic energy differences increase. For $\Delta E_{el} = 0.25$ there are at least two components in dynamics, a faster one with transition times τ_1 of ~11 ps and a slower one with $\tau_2 \approx$ 48 ps, which, at $\Delta E_{el} = 0.4$ eV, are shifted at longer times: $\tau_1 \approx 25$ ps; $\tau_2 \approx 95$ ps. In the case of $\Delta E_{el} = 0.62$ eV, the transition becomes much slower, the first peak occurring after ~100 ps.

The computed transition times are all of the same order of magnitude of the observed ET rates (200 ps at 25 K, 60 ps at 50 K) (41). Because of uncertainties both on the values of the electronic energy difference and coupling element and on the nature of the initial state (Franck-Condon or Boltzmann population), a more stringent comparison between computed and observed transition times is not possible at this stage; the fit of the best electronic parameters and of the temperature dependence of ET rates are out of the scopes of this article; work is in progress along these lines.

In the case of $\Delta E_{el} = 0.25$ eV there are always a couple of leading states in dynamics, exhibiting a significantly higher probability than all the other states. It is usually sufficient to change ΔE_{el} by a tiny amount (5 cm^{-1}) for changing the leading vibrational state for the transition. That behavior is easily understood by looking at Fig. 1 *c*, which shows that there are several vibrational states that are comparatively more strongly coupled to the initial state, so that each of them will be the leading one in a tiny energy interval. All the active modes used in dynamics are involved, at least once, in a leading state, of course in combination with other active modes, but there are a few modes that recur more times: the two low-frequency displaced modes of BPh (135 and 146 cm^{-1}) and that of Q_A^{-} at 473 cm^{-1}, the only mode that is recurrently populated with more than one quantum. Moreover, because of the high ΔE_{el} for ET (42), all the high-frequency displaced modes of Q_A^{-}, at 1174, 1545, and 1643 cm^{-1}, play an important role in ET dynamics, and, to a lesser extent, the mode at 1184 cm^{-1} of BPh too.

The vibrational modes that are important in ET dynamics performed at $\Delta E_{el} = 0.4 \pm 3.1\ 10^{-3}$ eV are substantially unchanged, but for the fact that a couple of slightly displaced modes of Q_A^{-} (318 and 367 cm^{-1}) have to be included as

active modes to have transition probabilities near to unity. The increase of the active space is necessary for balancing the decrease of the FC integrals as the energy gap between the initial and final state increases. As a result, the number of the final states that are populated in the transition significantly increases, from 10 to 15 for $\Delta E_{el} = 0.25$ eV to 50–60 for $\Delta E_{el} = 0.40$ eV; in some dynamics, those that exhibit lower probabilities (25–30%), no leading state is found in the time evolution of the wavefunction. If the electronic coupling element is set to 10 cm^{-1}, the transition probabilities are roughly one-third of those obtained previously (see Fig. 4) and transition times increase, staying, however, within the limits of the observed ET rates. Transition probabilities are still high enough, at least in the cases of $\Delta E_{el} = 0.25$ and 0.4 eV, to claim that intramolecular modes are sufficient for promoting ET.

DISCUSSION AND CONCLUSIONS

The results discussed so far indicate that ET from BPh^- to Q_A can be theoretically modeled as a nonradiative transition that mainly involves the intramolecular modes of vibrations of the two redox cofactors, without the assistance of the low-frequency modes of the medium. That conclusion is in good agreement with the general finding that most of the ET processes occurring in photosynthetic reaction centers ($P^* \rightarrow BPh, BPh^- \rightarrow Q_A, Q_A^- \rightarrow P^+$) shows only modest dependence of their rates from temperature (43,44,15,16,45). For ET from BPh^- to Q_A (16), the analysis of the ET rates of 22 quinone reconstituted RCs, covering a range of ΔG^0 from 0.2 to 0.8 eV and a range of T from 10 to 298 K, can lead us to suggest that ET from BPh^- to Q_A is not promoted by the low energy vibrations of the medium, which can be treated classically, but rather by discrete vibrations, whose energy spacing is larger than k_bT.

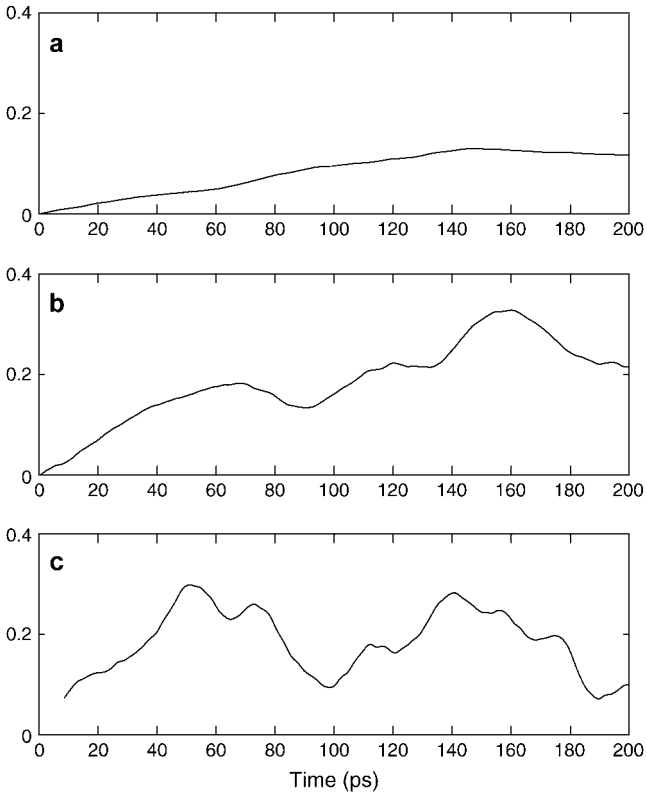

FIGURE 4 Transition probabilities of ET from pheophytin to ubiquinone: $\Delta E_{el} = 0.62$ eV (*a*), 0.40 eV (*b*), 0.25 eV (*c*); electronic coupling element: 10 cm^{-1}. Excited vibrations and maximum excitation numbers as in Fig. 3.

In isolated RCs of *Rhodopseudomonas sphaeroides* the rate of ET from BPh^- to Q_A show an unusual temperature dependence: the rate increases about threefold with decreasing temperature between 300 and 25 K, and decreases of about the same amount below 25 K (41). Attempts to fit the temperature dependence of ET rates, by using the Fermi golden rule expression and ad hoc estimates of normal mode displacements and frequencies (41), showed that the simplest and most successful model for ET would imply at least two soft modes (50 and 10 cm^{-1}) and a quantum mode at 400 cm^{-1}. Indeed, according to our results the most important mode in ET dynamics is the mode at 473 cm^{-1} of Q_A^-. Moreover, the two soft modes necessary to fit the temperature dependence of ET rates could be provided by the two low-frequency vibrations of neutral Q_A, falling at 24 and 42 cm^{-1}, which are both significantly displaced to play a role in ET (cf. Table 1) but further studies are necessaries to better asses how these very low-frequency modes are altered by the interaction with the protein matrix. Furthermore, the assumption made by Schenck et al. of a much smaller ΔE_{el}, 390 cm^{-1}, than that found by delayed fluorescence measurements (42), is not necessary because ET is significantly coupled also to high-frequency modes, both of BPh and of Q_A, which can account for the larger electronic energy difference.

The assumption that thermal motion causes slight fluctuations of the electronic energy difference around its mean value allows us to obtain transition probabilities and transition times that are stable with respect to small change of ΔE_{el}, an important point in a discrete state approach. Thus, a physical model in which the surrounding medium accounts for small energy fluctuations, due to weak interactions of the two redox partners with their environment, rather than directly providing coupled modes, can correctly reproduce at least the order of magnitude of ET rates in this specific case of ET from BPh^- to Q_A. Stronger effects of the surrounding medium will probably occur on a longer timescale than ET, thus being mainly responsible for energy dissipation. In the case of ET from BPh^- to Q_A, it is in fact experimentally well established that Q_A^- is significantly stabilized by the formation of a strong H-bond with the adjacent iron-histidine (11), as is also supported by theoretical computations (9). However, our results would indicate that this effect, deliberately not included, is not crucial for ET dynamics.

The importance of energy fluctuations also emerges from recent work on charge recombination from Q_A^- to the special pair (46,47). The analysis of ET rates between 10 and 300 K by the spin-boson model (48) leads to a significant broader energy gap distribution than that used in this article. This is not surprising, because $P^+Q_A^-$ charge recombination takes place in hundreds of milliseconds, and it is reasonable to assume that this long time is due to conformational changes in the protein, leading to the optimum conformation for the radiationless transition. In the case treated here, the very tiny energy gap distribution reflects the fact that ET is faster, and therefore there is no time for a large sampling of the conformational space of the protein.

The above results have been obtained by neglecting the interactions of the redox cofactors with the atoms of protein matrix. That assumption could affect: i), the vibrational frequencies of the low-frequency modes; ii), the equilibrium configurations of the redox cofactors; iii), the localized character of the low-frequency modes of the two cofactors. The first point is of little importance for ET dynamics, because the couplings between initial and final states mainly depend on the displacements of normal coordinates rather than on frequency changes upon ET. Frequency changes could also affect ET dynamics by adding or removing accidental degeneracy that could drive ET, but in the case we are dealing with there are so many coupled states (cf. Fig. 1, *b* and *c*) that a slight variation of one or more frequencies cannot substantially change the results. As concerns point ii, the computed displacements of normal coordinates are small in this case (the maximum displacement for the ubiquinone mode falling at 460 cm^{-1} is ~0.4 Å a.m.u.$^{1/2}$, which roughly means 0.13 Å ''linear'' displacement of the whole molecule), so that it is reasonable to assume that such a tiny movement cannot be hampered by van der Waals contacts with the protein matrix. As concerns the last point, Czarnecki et al. (49) have found that the resonance Raman spectra of bacterial RCs in which BClh and BPh cofactors were isotopically marked, exhibit low-frequency signals that are sensitive to isotopic labeling. That is strong evidence of the intramolecular character of these modes. In that article other very low-frequency modes were assigned to intramolecular vibrations. Time-resolved pump-probe spectroscopy (50) also indicated that the low-frequency vibrations coupled to the initial ET from the special pair are predominantly from intramolecular modes of histidine-ligated BClh macrocycles. However, there are also different points of view; the observation of changes in the low-frequency region observed in mutants (51) has led to the conclusion that the lowest-frequency modes important for the initial ET from the special pair are protein-cofactor intermolecular modes. Thus, the question about the intra- or intermolecular character of the low-frequency modes is still open; theoretical work aimed to better address this point is in progress.

The main conclusion, i.e., that long-range ET can take place without the assistance of the low-frequency modes of the medium, of course, holds for the specific case of ET from BPh^- to Q_A in bacterial photosynthetic RCs, but analyses such as that used here (see also Reimers and Hush (52)) starting from the knowledge of the intramolecular modes of vibrations of the two redox cofactors, can be also useful for a better understanding of cases where the embedding medium plays a major role. For instance, in a previous article we have shown that for ET from primary to secondary quinone intermolecular modes are necessary, because the Franck-Condon weighted density of states, as obtained by the intramolecular modes alone, is too low to give high ET probabilities (see also Fig. 2 for appreciating the huge difference between these two long-range ET processes) (38). Hopefully, longstanding problems in long-range ET in proteins, such as the debate concerning the existence or not of specific ET paths in proteins (53,54,55), could find a conclusive assessment when the role of intramolecular modes will be better established.

Computational details

Geometry optimizations and frequency computations have been carried out at DFT level, by using the B3LYP hybrid exchange-correlation potential (56), and the G94 package (57). All geometry optimization runs started from the x-ray coordinates of the RC from *R. sphaeroides* crystallized under illumination.(58,37) In the case of pheophytin, geometry optimizations were carried at DFT/B3LYP/6-31g* level, whereas for the determination of vibrational frequencies the smaller 3-21g basis set was used. In the case of ubiquinone, optimum geometries and frequencies were computed at DFT/B3LYP/6-31++g** level.

Franck-Condon factors have been computed by the MOLFC package (32).

The time evolution of the system initially prepared in the ground vibronic state of $|BPh^-Q_A\rangle$ has been determined by solving the time-dependent Schrödinger equation (cf. Eq. 9) employing the Lanczos algorithm (59). The manifold of final states has been pruned by considering only those states falling in a small energy interval (± 10 cm^{-1}) around the energy of the initial state. The convergence of the Lanczos procedure has been tested in several cases by performing dynamics using exact diagonalization of the Hamiltonian matrix in a reduced active space, chosen according to the results of the Lanczos propagation.

Because we are at the limits of computer capabilities ($>10^7$ states have been used in dynamics) the convergence of the results with the size of the active space cannot be properly addressed. The modes included in the active space and the number of states for each mode have been selected on the basis of several test computations, which indicate that there are other modes potentially important for ET.

The financial support of the University of Salerno is gratefully acknowledged.

REFERENCES

1. Voet, D., and J. Voet. 1995. Biochemistry. John Wiley and Sons, Hoboken, NJ.
2. Bendall, D. S. 1996. Protein Electron Transfer. Bios Scientific Publisher, Oxford, UK.
3. Marcus, R. A. 1956. On the oxidation-reduction reactions involving electron transfer. *J. Chem. Phys.* 24:966–978.
4. Hopfield, J. J. 1974. Electron transfer between biological molecules by thermal activated tunneling. *Proc. Natl. Acad. Sci. USA.* 71:3640–3644.
5. Kestner, N. R., J. Logan, and J. Jortner. 1974. Thermal electron transfer reactions in polar solvents. *J. Phys. Chem.* 78:2148–2166.
6. Sumi, H., and R. A. Marcus. 1986. Dynamical effects in electron transfer reactions. *J. Chem. Phys.* 84:4894–4914.
7. Di Valentin, M., A. Bisol, G. Agostini, M. Fuhs, P. A. Liddell, A. L. Moore, T. A. Moore, D. Gust, and D. Carbonera. 2004. Photochemistry of artificial photosynthetic reaction center in liquid crystals probed by multifrequency EPR (9.5 and 95 GHz). *J. Am. Chem. Soc.* 126:17074–17086.
8. Liddell, P. A., G. Kodis, L. de la Garza, A. L. Moore, and T. A. Moore. 2004. Benzene templated model systems for photosynthetic antenna-reaction centers function. *J. Phys. Chem. B.* 108:10256–10265.
9. Peluso, A., M. Di Donato, and G. A. A. Saracino. 2000. An alternative way of thinking about electron transfer in proteins: proton assisted electron transfer between the primary and secondary quinones in photosynthetic reaction centers. *J. Chem. Phys.* 113:3212–3218.
10. Hung, S., A. N. McPherson, S. Lin, P. A. Liddell, G. R. Seely, T. A. Moore, and D. Gust. 1995. Coordinated photoinduced electron and proton transfer in a molecular triad. *J. Am. Chem. Soc.* 117:1657–1658.
11. Rohrer, M., F. MacMillan, T. F. Prisner, A. T. Gardiner, K. Mobius, and W. Lubitz. 1998. Pulsed ENDOR at 95 GHz on the primary acceptor ubisemiquinone Q_A^- in photosynthetic bacterial reaction centers and related model systems. *J. Phys. Chem. B.* 102:4648–4657.
12. Okamura, M. Y., M. Paddock, M. S. Graige, and G. Feher. 2000. Proton and electron transfer in bacterial reaction centers. *Biochim. Biophys. Acta.* 1458:148–163.
13. Markel, F., N. Ferris, I. Gould, and A. Myers. 1992. Mode-specific vibrational reorganization energies accompanying photoinduced electron transfer in the hexamethylbenzene/tetracyanoethylene charge-transfer complex. *J. Am. Chem. Soc.* 114:6208–6219.
14. Fischer, S. F., and R. P. Van Duyne. 1977. On the theory of electron transfer reactions. The naphtalene/TCNQ system. *Chem. Phys.* 26:9–16.
15. Gunner, M. R., D. E. Robertson, and P. L. Dutton. 1986. Kinetic studies on the reaction center protein from *Rhodobacter sphaeroides*: the temperature and the free energy dependence of electron transfer between various quinones in the Q_A site and the oxidized bacteriochlorophyll dimer. *J. Phys. Chem.* 90:3783–3795.
16. Gunner, M. R., and L. P. Dutton. 1989. Temperature and $-\Delta G^0$ dependence of the electron transfer from BPh^- to Q_A in reaction center protein from *Rhodobacter sphaeroides* with different quinones as Q_A. *J. Am. Chem. Soc.* 111:3400–3412.
17. Wegenwijs, B., and J. W. Verhoeven. 1999. Long-range charge separation in solvent free donor-bridge-acceptor systems. *Adv. Chem. Phys.* 106:221–264.
18. Paddow-Row, M. N. 1994. Investigating long-range electron transfer with rigid, covalently linked donor-(norbornylogous bridge)-acceptor systems. *Acc. Chem. Res.* 27:18–25.
19. Xie, A., F. G. v. d. M. Alexandre, and R. H. Austin. 2002. Excited-state lifetimes of far-infrared collective modes in proteins. *Phys. Rev. Lett.* 88:018102(1–4).
20. Moritsugu, K., O. Miyoshita, and A. Kidera. 2000. Vibrational energy transfer in a protein molecule. *Phys. Rev. Lett.* 85:3970–3973.
21. Borrelli, R., and A. Peluso. 2003. Dynamics of radiationless transitions in large molecular systems: a Franck-Condon based method accounting for displacements and rotations of all the normal coordinates. *J. Chem. Phys.* 119:8437–8448.
22. Robinson, G. W., and R. P. Frosch. 1962. Theory of electronic energy relaxation in solid phase. *J. Chem. Phys.* 37:1962–1973.
23. Bixon, M., and J. Jortner. 1999. Electron transfer: from isolated molecules to biomolecules. *Adv. Chem. Phys.* 106:35–203.
24. Alfano, D., A. Peluso, and R. Borrelli. 2002. A simple method for estimating activation energies of proton-transfer reactions. *J. Phys. Chem. A.* 106:7018–7025.
25. Mead, C. A., and D. G. Truhlar. 1979. On the determination of Born-Oppehneimer nuclear motion wave functions including complications due to conical intersections and identical nuclei. *J. Chem. Phys.* 70:2284–2296.
26. Ivashin, N., B. Kallebring, S. Larsson, and O. Hansson. 1998. Charge separation in photosynthetic reaction centers. *J. Phys. Chem. B.* 102 :5017–5022.
27. Duschinsky, F. 1937. On the interpretation of electronic spectra of polyatomic molecules. I. Concerning the Franck-Condon principle. *Acta Phisicochim. URSS.* 7:551–566.
28. Sharp, T. E., and K. M. Rosenstock. 1964. Franck-Condon factors for polyatomic molecules. *J. Chem. Phys.* 41:3453–3463.
29. Reimers, J. R. 2001. A practical method for the use of curvilinear coordinates in calculations of normal-mode-projected displacements and Duschinsky rotation matrices for large molecules. *J. Chem. Phys.* 115:9103–9109.
30. Peluso, A., F. Santoro, and G. Del Re. 1997. Vibronic coupling in electronic transitions with significant Duschinsky effect. *Int. J. Quantum Chem.* 63:233–244.
31. Doktorov, E. V., I. A. Malkin, and M. V. I. 1975. Dynamical symmetry of vibronic transitions in polyatomic molecules and the Franck-Condon principle. *J. Mol. Spec.* 56:1–20.
32. Borrelli, R., and A. Peluso. 2004. MolFC: a program for Franck-Condon integrals calculation. Available at http://pcdual.chem.unisa.it. [Online].
33. Kleinfeld, D., M. Y. Okamura, and G. Feher. 1984. Electron transfer kinetics in photosynthetic reaction center cooled to cryogenic temperature in the charge separated state: evidence for light-induced structural changes. *Biochemistry.* 23:5780–5786.
34. Franzen, S., and S. G. Boxer. 1993. Temperature dependence of the electric field modulation of electron transfer rates: charge recombination in photosynthetic reaction centers. *J. Phys. Chem.* 97:6304–6318.
35. McPherson, P. H., V. Nagarajan, W. W. Parson, M. Y. Okamura, and G. Feher. 1990. pH dependence of the free energy gap between DQ_A and $D^+Q_A^-$ determined from delayed fluorescence in reaction centers from *Rhodobacter sphaeroides* R-26. *Biochim. Biophys. Acta.* 1019: 91–94.
36. Breton, J., and E. Nabedryk. 1998. Proton uptake upon quinone reduction in bacterial reaction centers: IR signature and possible participation of a highly polarizable hydrogen bond network. *Photosynth. Res.* 55:301–307.
37. Stowell, M. H. B., T. McPhillips, D. C. Rees, S. M. Soltis, E. Abresch, and G. Feher. 1997. Light induced structural changes in photosynthetic reaction center: implications for mechanism of electron-proton transfer. *Science* 276:812–816. PDB ID: 1AIG.
38. Di Donato, M., A. Peluso, and G. Villani. 2004. Electron transfer between quinones in photosynthetic reaction centers. *J. Phys. Chem. B.* 108:3068–3077.
39. Almeida, R., and R. A. Marcus. 1990. Dynamics of electron transfer for a nonsuperexchange coherent mechanism. 2. Numerical calculations. *J. Phys. Chem.* 94:2978–2985.
40. Kuhn, H. 1986. Electron transfer mechanism in the reaction center of photosynthetic bacteria. *Phys. Rev. A.* 34:3409–3425.
41. Schenck, C. C., W. W. Parson, D. Holten, M. W. Windsor, and A. Sarai. 1981. Temperature dependence of electron transfer between bacteriopheophytine and ubiquinone in protonated and deuterated

reaction centers of *Rhodopseudomonas sphaeroides*. *Biophys. J.* 36: 479–489.

42. Woodbury, W. T., and W. W. Parson. 1984. Nanosecond fluorescence from isolated photosynthetic reaction centers of *Rhodopseudomonas sphaeroides*. *Biochim. Biophys. Acta*. 767:345–361.
43. Woodbury, N. W. T., N. Becker, D. Middendorf, and W. W. Parson. 1985. Picosecond kinetics of the initial photochemical electron-transfer reaction in bacterial photosynthetic reaction centers. *Biochemistry*. 24:7516–7521.
44. Kirmaier, C., D. Holten, and W. W. Parson. 1985. Temperature and detection-wavelength dependence of the picosecond electron transfer kinetics measured in *Rhodopseudomonas sphaeroides* reaction centers. Resolution of new spectral and kinetic components in the primary charge separation process. *Biochim. Biophys. Acta*. 810:33–48.
45. McElroy, J. D., D. C. Mauzerall, and G. Feher. 1974. Characterization of primary reactants in bacterial photosynthesis. II. Kinetics studies of the light induced signal ($g = 2.0026$) and the optical absorbance changes at cryogenic temperatures. *Biochim. Biophys. Acta*. 333: 261–278.
46. Kriegl, J. M., and G. U. Niehaus. 2004. Structural, dynamic, and energetic aspects of long-range electron transfer in photosynthetic reaction centers. *Proc. Natl. Acad. Sci. USA*. 101:123–128.
47. Kriegl, J. M., F. K. Forster, and G. U. Nienhaus. 2003. Charge recombination and protein dynamics in bacterial photosynthetic reaction centers entrapped in a sol-gel matrix. *Biophys. J.* 85:1851–1870.
48. Xu, D., and K. Schulten. 1994. Coupling of protein motion to electron transfer in a photosynthetic reaction center: investigating the low temperature behavior in the framework of the spin-boson model. *Chem. Phys.* 182:91–117.
49. Czarnecki, K., J. R. Diers, V. Chynwat, J. P. Erickson, H. A. Frank, and D. F. Bocian. 1997. Characterization of the strongly coupled, low-frequency vibrational modes of the special pair of photosynthetic reaction centers via isotopic labeling of the cofactors. *J. Am. Chem. Soc*. 119:415–426.
50. Shelly, K. R., E. A. Carson, and W. F. Beck. 2003. Vibrational coherence from the dipyridine complex of bacteriochlorophyll *a*: intramolecular modes in the 10–220-cm^{-1} regime, intermolecular solvent modes, and relevance to photosynthesis. *J. Am. Chem. Soc.* 125:11810–11811.
51. Rischel, C., D. Spiedel, J. P. Ridge, M. R. Jones, J. Breton, J.-C. Lambry, J.-L. Martin, and M. H. Vos. 1998. Low frequency vibrational modes in proteins: changes induced by point-mutations in the protein-cofactor matrix of bacterial reaction centers. *Proc. Natl. Acad. Sci. USA*. 95:12306–12311.
52. Reimers, J. R., and N. S. Hush. 2004. A unified description of the electrochemical, charge distribution, and spectroscopic properties of the special-pair radical cation in bacterial photosynthesis. *J. Am. Chem. Soc*. 126:4132–4144.
53. Beratan, D. N., J. N. Betts, and J. N. Onuchic. 1991. Protein electron transfer rates set by the bridging secondary and tertiary structure. *Science* 252:1285–1288.
54. Beratan, D. N., J. N. Onuchic, J. R. Winkler, and H. B. Gray. 1992. Electron tunneling pathways in proteins. *Science*. 258:1740–1741.
55. Page, C. C., C. C. Moser, X. Chen, and P. L. Dutton. 1999. Natural engineering principles of electron tunnelling in biological oxidation-reduction. *Nature*. 402:47–52.
56. Lee, C., W. Yang, and R. G. Parr. 1988. Development of the Colle-Salvetti correlation-energy formula into a functional of the electron density. *Phys. Rev. B*. 37:785–789.
57. Frisch, M. J., G. W. Trucks, H. B. Schlegel, P. W. Gill, B. G. Johnson, M. A. Robb, J. R. Cheeseman, T. Keith, G. A. Petersson, J. A. Montgomery, K. Raghavachari, M. A. Al-Laham, et al. 1995. Gaussian 94, Revision C.2. Gaussian Inc., Pittsburgh, PA.
58. Berman, H. M., J. Westbrook, Z. Feng, G. Gilliland, T. N. Bhat, H. Weissig, I. N. Shindyalov, and P. E. Bourne. 2000. The protein data bank. *Nucleic Acids Res.* 28:235–242.
59. Park, J. T., and J. C. Light. 1986. Unitary quantum time evolution by iterative Lanczos reduction. *J. Chem. Phys.* 85:5870–5876.
60. Beyer, T., and D. F. Swinehart. 1973. Number of multiply restricted partitions. *Commun. Assoc. Comput. Machin.* 16:379.
61. Stein, S. E., and B. S. Rabinovitch. 1973. Accurate evaluation of internal energy level sums and densities including anharmonic oscillators and hindered rotors. *J. Chem. Phys.* 58:2438–2445.